The Journal of Chemical Physics ARTICLE scitation.org/journal/jcp

Vapor sorption in binary polymer brushes: The effect of the polymer–polymer interface

Cite as: J. Chem. Phys. 155, 054904 (2021); doi: 10.1063/5.0057065
Submitted: 17 May 2021 • Accepted: 23 July 2021 •
Published Online: 4 August 2021

Leon A. Smook, Guido C. Ritsema van Eck, and Sissi de Beer[a)]

AFFILIATIONS

Sustainable Polymer Chemistry Group, Department of Molecules and Materials, MESA+ Institute for Nanotechnology, University of Twente, P.O. Box 217, 7500 AE Enschede, The Netherlands

[a)]Author to whom correspondence should be addressed: s.j.a.debeer@utwente.nl

ABSTRACT

Polymer brushes attract vapors that are good solvents for polymers. This is useful in sensing and other technologies that rely on concentrating vapors for optimal performance. It was recently shown that vapor sorption can be enhanced further by incorporating two incompatible types of polymers A and B in the brushes: additional vapor adsorbs at the high-energy polymer–polymer interface in these binary brushes. In this article, we present a model that describes this enhanced sorption in binary brushes of immiscible A–B polymers. To do so, we set up a free-energy model to predict the interfacial area between the different polymer phases in binary brushes. This description is combined with Gibbs adsorption isotherms to determine the adsorption at these interfaces. We validate our model with coarse-grained molecular dynamics simulations. Moreover, based on our results, we propose design parameters (A–B chain fraction, grafting density, vapor, and A–B interaction strength) for optimal vapor absorption in coatings composed of binary brushes.

I. INTRODUCTION

Polymers can be end-grafted to surfaces, and they form polymer brushes[1,2] when the average distance between the anchor points is smaller than their radius of gyration. These polymers can change the surface properties of coated materials,[3,4] from reducing friction[5] to introducing anti-fouling behavior.[6,7] Moreover, brush coatings allow for a remarkable freedom in surface functionalization—much of the toolbox of polymer chemistry is available for these coatings as well.[8] Polymer brushes are especially interesting for sensing applications:[9–11] brushes can be functionalized with moieties to enable sensing specific molecules.[12,13] For instance, polymer brushes have been functionalized with antibodies using click chemistry, leading to a fouling-resistant sensor surface that is specific to a model analyte.[14,15] As such, polymer brush-based sensors form a promising tool for point-of-care diagnostic devices.

By using the intrinsic responsiveness of polymers to their environments,[16,17] bare brushes without special functional groups can also prove to be useful in sensing applications, especially in gaseous media.[18–20] The sensitivity of most vapor sensor platforms, for example, capacitive, gravimetric, or optical sensors, depends strongly on the amount of vapor molecules that can be attracted to the sensor surface.[21] Brushes are excellent surface functionalizations to concentrate the vapors near the sensor surface[18–20] since they can absorb solvent vapors. The amount of absorption depends on the chemical makeup of the brush and the vapor, which has been observed experimentally[22–28] and in simulations.[29,30]

In a recent article,[31] we showed that the creation of high-energy interfaces between nanodomains in binary brushes can enhance the sorption of vapor compared to similar homopolymer brushes and bare attractive surfaces. Such binary polymer brushes[32,33] consist of different polymers anchored to the same surface and can be prepared by commonly employed synthesis strategies.[34–36] In brushes in which polymer cross-interactions are less favorable than polymer self-interactions, nanodomains are rich in either polymer form. The interfaces between these nanodomains provide additional high-energy surfaces where vapor can adsorb.

Nevertheless, evaluating the interfacial area between these different polymer domains is a non-trivial exercise. The morphological properties of these brushes are governed by the properties of the polymer and their anchoring: polymer fraction, cross-interaction strength,[37] anchoring[38] and annealing conditions,[39] solvent treatment,[40] temperature,[41] and functionalization[42,43] all affect the morphology of these mixed brushes. Therefore, there is a need to

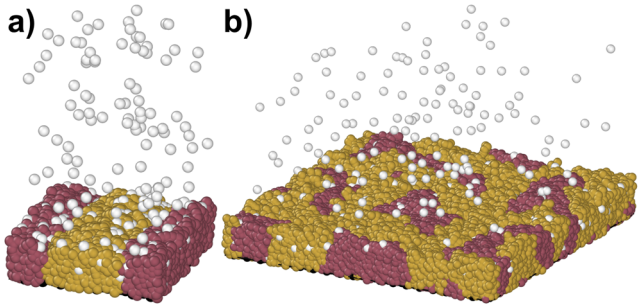

FIG. 1. Snapshot of a striped brush (a) and a mixed brush (b), both with a chain fraction ϕ of 0.5 as used in the simulations in this work. The red and yellow particles illustrate the different polymer type and the white particles illustrate the vapor.

evaluate this polymer–polymer surface area in order to estimate the additional sorption in these brushes. This will allow one to find the optimal design parameters of the brush.

In this article, we show how vapor absorption in mixed brushes is affected by the design parameters of these coatings, i.e., grafting density, polymer chain fractions, and interaction strengths. To gain insight into the adsorption at the polymer–polymer interfaces in binary brushes, we study the adsorption of vapor at well-defined polymer–polymer interfaces in striped brushes [Fig. 1(a)] with coarse-grained molecular dynamics simulations and link this to the Gibbs adsorption isotherm. In mixed brushes, these interfaces are less well-defined though [Fig. 1(b)]. Therefore, we also develop a model to estimate the interfacial area in a mixed brush based on free energies in the system. Then, we perform molecular dynamics simulations on mixed brushes in which we systematically vary the grafting density, chain fraction, and interaction strengths. Finally, we compare the sorption characteristics of these mixed brushes with the adsorption theory and our free-energy model. We find that the vapor sorption at the polymer–polymer interface follows the Gibbs adsorption isotherm, that our free-energy model can predict the interfacial area, and that the interfacial properties depend strongly on the properties of the binary brush and the interactions of its components with the vapor. Based on these results, we propose design rules to optimize vapor sorption in mixed brushes.

II. THEORY

A. Adsorption at interfaces

Adsorption at interfaces can be described by the Gibbs adsorption isotherm. This expression reads in its differential form,

$$d\gamma = -\sum_i \Gamma_i d\mu_i, \tag{1}$$

where γ is the interfacial tension, Γ is the surface excess (equivalent to vapor sorption at the interface), and μ is the chemical potential of the adsorbing species. The index i loops over all adsorbing species. Here, we expose binary polymer brushes to a mono-component vapor with a varying vapor pressure. The chemical potential of this vapor reads

$$\mu = \mu_0 + kT \ln\left(\frac{f}{p_{\text{sat}}}\right), \tag{2}$$

where kT is the thermal energy; f is the fugacity, which is a direct measure of the molar Gibbs internal energy (it is imposed by the chemostat in our simulations);[44] and p_{sat} is the saturation pressure of the vapor. In its differential form, the standard chemical potential (μ_0) drops out of the equation. Combining Eqs. (1) and (2) provides the following differential expression:

$$d\gamma = -kT\,\Gamma d \ln\frac{f}{p_{\text{sat}}}. \tag{3}$$

Hence, the surface excess can be estimated by looking at the response of the surface tension as a function of the relative vapor pressure.

B. Model for the polymer–polymer interface

In striped brushes [Fig. 1(a)], it is straightforward to determine the interfacial area from the simulation parameters. We simply estimate the height of the interface and multiply it with the width of the box in the direction parallel to the stripe. Yet, for mixed brushes [Fig. 1(b)], this is difficult because they can exhibit morphologically different phases depending on their properties such as grafting density, grafting fraction, and the chemical nature of the polymers. In previous self-consistent field theory calculations,[45,46] several separated phases have been identified in mixed brushes: (I) a half-sphere phase, (II) a cylindrical phase, and (III) a ripple phase, as schematically depicted in Fig. 2.

These different phases impact the adsorption of a vapor by modifying the contact area between different polymer types. Here, we describe these different phases from a free energy perspective to determine the thermodynamically stable phase. For each phase, we describe the free energy based on enthalpic and entropic contributions. Below, we derive this model for mixed brushes of polymers with equal properties (length and interaction with vapor) but with an un-favorable cross-interaction.

The different mixed phases can be evaluated by describing the free energy based on interfacial interactions and polymer chain stretching. In broad terms, this gives

$$\Delta F_u = \frac{A\gamma}{S} + \rho\phi\frac{3}{2N}L_A^2 + \rho(1-\phi)\frac{3}{2N}L_B^2, \tag{4}$$

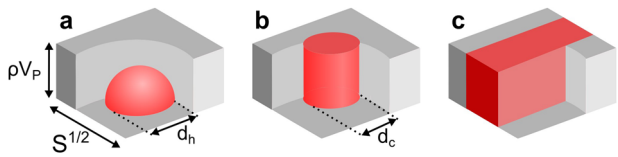

FIG. 2. Schematic representation of the different brush phases: (a) a half-sphere phase, (b) a cylindrical phase, and (c) a ripple phase. The area depicted corresponds to S, the area within which all minority chains aggregate into a single domain. The different polymers are indicated with the red and gray colors.

where A is the interfacial area, γ is the surface tension, ρ is the grafting density, ϕ is the grafting fraction, L_A and L_B are the stretching lengths of the different chain types, and S is the area associated with a domain. In other words, S is the smallest area within which all minority chains aggregate into a single domain. To find the free energy of a phase, we simply minimize this expression with respect to S for a given γ, ρ, and ϕ. The values of A, L_A, and L_B follow directly from the other parameters [S, ρ, ϕ_A, ϕ_B, and the volume per polymer (V_p)] as described below.

The interfacial area A between different nanophases follows from the geometry and the number of chains associated with an area S. If we define an area S and assume that all minority chains in this area coalesce in a single domain, we can express the interfacial area associated with this domain. The volume of the minority phase follows from

$$V = S\rho\phi V_p. \tag{5}$$

Depending on the geometry of the minority phase (either half-sphere, cylinder, or stripe) and assuming a homogeneous brush height, the interfacial area associated with this minority phase is

$$A = \frac{\pi}{2}\left(\frac{12}{\pi}V\right)^{2/3} \quad \text{(hemisphere)}, \tag{6}$$

$$A = \sqrt{4\pi\rho V_p V} \quad \text{(cylinder)}, \tag{7}$$

$$A = 2\rho V_p S^{1/2} \quad \text{(stripe)}. \tag{8}$$

We can also define the stretching energy of the chains in each of these phases. We assume Gaussian chain stretching [see quadratic terms in Eq. (4)], and take into account the length scales in each phase, we get for the minority phase,

$$L_A = S^{1/2}/2 \quad \text{(hemisphere)}, \tag{9}$$

$$L_A = \sqrt{(\rho V_p)^2 + (S^{1/2}/2)^2} \quad \text{(cylinder)}, \tag{10}$$

$$L_A = \sqrt{(\rho V_p)^2 + (\phi(S^{1/2}))^2} \quad \text{(stripe)}, \tag{11}$$

and for the majority phase,

$$L_B = \sqrt{(\rho V_p)^2 + (d_h/2)^2} \quad \text{(hemisphere)}, \tag{12}$$

$$L_B = \sqrt{(\rho V_p)^2 + (d_c/2)^2} \quad \text{(cylinder)}, \tag{13}$$

$$L_B = \sqrt{(\rho V_p)^2 + ((1-\phi)(S^{1/2}))^2} \quad \text{(stripe)}. \tag{14}$$

Note that these lengths, in general, contain two contributions: one perpendicular to the grafting surface (related to the brush height) and the other parallel to the grafting surface (related to the characteristic size of a domain). This description of the chain length follows a similar principle as described in earlier work.[47,48] The remaining parameter in this model is the surface tension (γ), which can be extracted from the stripe brush simulations.

We then use Eqs. (6)–(14) in Eq. (4) and minimize this expression with respect to S to find the free energy of the phase normalized by the grafting area. Finally, the phase with the lowest free energy is chosen and the interfacial area is evaluated for that phase.

III. MODEL AND METHODS

A. Molecular dynamics simulation setup

We simulate brushes consisting of end-grafted polymers of two different types, A and B. These polymers are modeled as Kremer–Grest chains[49] with 30 beads. Chains of this length have shown qualitative agreement with experimental work, for example, in friction measurements.[50–52] Entanglements cannot be formed with these short polymers. Yet, we anticipate that entanglements will have only a minor effect on vapor adsorption between nanodomains, since they are not expected to exist over domain boundaries. The chains are anchored onto a hexagonal lattice with a varying grafting density ρ (ranging from 0.05 to $0.35\sigma^{-2}$) in a box of ~$75 \times 75 \times 51\sigma^3$; the in-plane box dimensions are adapted to fit an integer number of unit cells, preserving the hexagonal lattice structure across the periodic boundary. For context, 1σ in our simulations corresponds to < 1 nm in real systems, so the simulated system spans an area smaller than 75×75 nm^2. The box edges perpendicular to the grafting surface are modeled with periodic boundary conditions. The grafting surface and upper wall are modeled with fixed boundary conditions and are enforced using a repulsive harmonic potential with a spring constant of $100\varepsilon\sigma^{-2}$. Chains of different types (A and B) are distributed randomly across the grafting points with a fraction of the minority chain ϕ ranging from 0 to 0.5 forming a mixed brush [see Fig. 1(b)].

To gain insight into the sorption at the polymer–polymer interfaces, we perform MD simulations on striped brushes with a well-defined interface; the anchor points of different chain types are spatially segregated [see Fig. 1(a)]. All parameters are equal to those of the mixed brushes, yet different vapor pressures and a smaller box of $30 \times 30 \times 51\sigma^3$ are used. Additionally, for both systems, a single-component brush ($\phi = 0$) is simulated to enable correction for bulk sorption.

Interactions between all nonbonded particle types (polymers A and B and vapor S) are modeled using a 12-6 Lennard-Jones potential,

$$U_{\mathrm{LJ}}(r) = 4\varepsilon\left(\left(\frac{\sigma}{r}\right)^{12} - \left(\frac{\sigma}{r}\right)^{6}\right), \tag{15}$$

$$U_{\mathrm{LJ,PS}}(r) = \begin{cases} U_{\mathrm{LJ}}(r) - U_{\mathrm{LJ}}(r_c) & \text{for } r \le r_c, \\ 0 & \text{for } r > r_c, \end{cases} \tag{16}$$

where r is the interparticle distance, σ is the point of zero crossing of the Lennard-Jones potential, and ε is the absolute value of the minimum of the 12-6 Lennard-Jones potential and where a cut-off distance (r_c) of 2.5σ is used. Bonded interactions are described by a combination of a finite extensible non-linear elastic (FENE) potential and a Weeks–Chandler–Anderson (WCA) potential such that

$$U_{\mathrm{FENE}}(r) = -0.5KR_0^2 \ln\left(1 - \left(\frac{r}{R_0}\right)^2\right), \tag{17}$$

$$U_{\mathrm{WCA}}(r) = \begin{cases} U_{\mathrm{LJ}}(r) + \varepsilon & \text{for } r \le 2^{1/6}\,\sigma, \\ 0 & \text{for } r > 2^{1/6}\,\sigma, \end{cases} \tag{18}$$

$$U_{\mathrm{bond}}(r) = U_{\mathrm{FENE}}(r) + U_{\mathrm{WCA}}(r). \tag{19}$$

Here, the parameters K, R_0, ε, and σ have values of $30\,\varepsilon\sigma^{-2}$, $1.5\,\sigma$, 1, and 1, respectively. This choice of parameters prevents non-physical behavior and bond crossing.[49]

Simulations are performed at a reduced temperature of $0.85\ \varepsilon k_B$, a temperature at which vapor–liquid coexistence is possible. This temperature is maintained using a train of three Nosé–Hoover thermostats with a damping coefficient of 0.15τ. This setup allows complete sampling of the NVT ensemble[53] and unaffected diffusion of vapor from the reservoir region into the brush.

Time integration is performed using a two-level rRESPA algorithm[54] with a small time step of $0.0075\,\tau$ and a large time step of $0.015\,\tau$. Bonded interactions are computed in the small time step, and pair forces are computed in the large time step. The vapor is introduced in the simulation using an alternating grand-canonical Monte Carlo–molecular dynamics (GCMC-MD) procedure as described in previous work.[29] In short, vapor particles are inserted/deleted every 10 000th time step according to the Metropolis criterion. Particle insertion via a Metropolis criterion allows for simulation of large virtual reservoirs without the need to explicitly simulate all particles in this reservoir. Too infrequent insertion/deletion of particles can result in density fluctuations.[55] However, we ensured that insertions/deletions every 10 000 time steps is frequently enough to prevent significant density fluctuations in the vapor phase after system equilibration. The simulation is performed in NVT for all other time steps. Simulations are performed using the LAMMPS software package.[56]

B. Surface tension and sorption in striped brushes

The simulation of striped brushes consists of three phases: (1) energy minimization using the conjugate gradient method to relax the initial configuration to a more natural state, (2) short dynamic equilibration in NVT for 50 000 time steps with a Langevin thermostat (damping 100 τ) to bring all particles to the correct velocities, and (3) long equilibration without and with a Lennard-Jones vapor (10 M time steps each). The equilibration was considered to be completed when the system had fully collapsed and the chains fully separated into the different phases. This is confirmed with the data files of the simulations, in which the polymer density profiles and solvent particle counts fluctuate around an equilibrium value and no longer display a systematic drift. During the production run, solvent density profiles are collected as well as the surface tension of the polymer–polymer interface. The quantity $p_N - p_T$, the difference in the pressure components in the directions parallel and perpendicular to the interface, is averaged over the height from $z = 0.05$–6.0σ and along the direction of the stripes. The surface tension is then estimated by integrating the difference between this quantity and a baseline corresponding to its minimum value (for details, see the supplementary material, Sec. 1). The sorption associated with the polymer–polymer interfaces is estimated by subtracting the sorption of a pure brush ($\phi = 0$) with similar properties under similar conditions from the sorption of the striped brush.

C. Sorption in mixed brushes

Simulations on mixed brushes were performed using a similar procedure compared to the striped brushes (for simulation details, see the supplementary material, Sec. 2). During the production run, we collect two-dimensional solvent and polymer density profiles and particle location at intervals of 50 000 time steps. To evaluate the sorption behavior of mixed brushes, we perform four experiments in which we systematically vary one of the following parameters: grafting density, grafting ratio, relative self-interaction, and relative polymer–vapor interaction. The system and interaction parameters for each of these experiments are tabulated in Table I. For each of these systems, we evaluate the vapor sorption.

IV. RESULTS AND DISCUSSION

We perform molecular dynamics simulations on striped brushes with well-defined interfaces in order to relate the sorption to the interfacial area and surface tension: These properties are more easily extracted from such well-defined interfaces. We then perform molecular dynamics simulations on mixed polymer brushes with varying properties. The properties of these brushes (i.e., chain fraction, grafting density, relative interaction strengths) are varied systematically and the brushes are exposed to a Lennard-Jones vapor at a relative vapor pressure of 30%. Finally, we compare the results of the simulations with our model.

A. Adsorption at interfaces

Surface tension is a main characteristic of interfaces. Figure 3 shows the interfacial surface tension as a function of the

TABLE I. Description of simulation experiments. The parameter that is evaluated in an experiment is not changed during the simulation, rather multiple simulations are run with different values for this parameter.

No.	ρ	ϕ	ε_{AB}	$\varepsilon_{AA}\|\varepsilon_{BB}$	$\varepsilon_{AS}\|\varepsilon_{BS}$	f/p_{sat} (%)
1	0.25	0.0–0.5	0.45	1.0|1.0	1.0|1.0	30
2	0.05–0.35	0.5	0.45	1.0|1.0	1.0|1.0	30
3	0.25	0.5	0.45	0.6–1.4|0.6–1.4	1.0|1.0	30
4	0.25	0.5	0.45	1.0|1.0	0.6–1.4|0.6–1.4	30

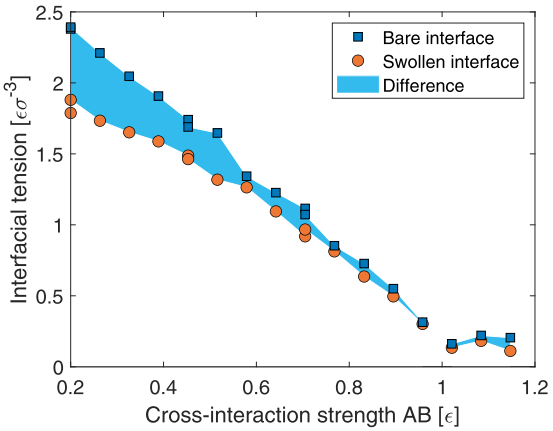

FIG. 3. Interfacial tension as a function of the polymer cross-interaction strength ε_{AB}. A weaker cross-interaction strength leads to a higher interfacial tension. The interfacial tension of an interface with vapor is lower than that of a "dry" interface, as expected based on the Gibbs isotherm.

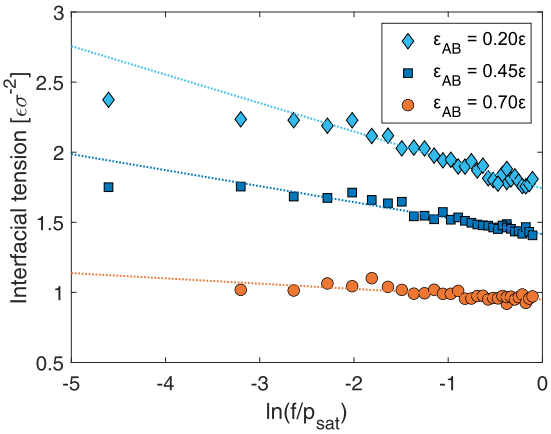

FIG. 4. Adsorption isotherms for interfaces with different cross-interaction strengths. The dotted lines indicate the fit of the Gibbs isotherm for each interface where the slope is proportional to $kT\Gamma$. A weaker cross-interaction strength leads to a higher surface excess Γ.

cross-interaction strength in striped brushes. The weaker the cross-interaction strength, the higher the surface tension becomes. Effectively, monomers near the interface experience a stronger interaction with particles on their side of the interface than with the particles on the other side. As a result, an inward force is acting on the particles. This force increases when the interaction with particles on the other side of the interface (in this case, ε_{AB}) decreases, resulting in a higher surface tension. Additionally, the surface tension decreases when vapor adsorbs at the interface (orange circles) as compared to a "dry" interface (blue squares); this decrease is shown with the blue shaded area. This observation is in qualitative agreement with the Gibbs adsorption [Eq. (1)] isotherm since a surface excess results in a decrease in the surface tension. Intuitively, this decrease is the result of vapor particles that reside at the interface. These particles interact well with both phases and, therefore, act as a glue between them, reducing the inward force acting on the monomers and, therefore, the surface tension.

If we vary the vapor pressure in this system, we obtain an adsorption isotherm. Figure 4 displays adsorption isotherms for striped brushes with different cross-interaction strengths on a semi-logarithmic plot. We observe that the adsorption behavior follows a linear trend in this semi-logarithmic plot, which is in line with the differential expression of the Gibbs adsorption isotherm. From these isotherms, we can extract the value of Γ by fitting a linear curve to the data (indicated with the dotted lines). We find a value for Γ of, respectively, $0.045, 0.134$, and $0.239\sigma^{-2}$ for cross-interaction strengths of $0.7, 0.45,$ and 0.2ε. Hence, we find that the excess sorption depends strongly on the energy associated with the interface of a dry brush.

The surface excess recovered from the isotherms should be equivalent to the additional sorption in the striped brushes. Figure 5 displays the surface excess as a function of the cross-interaction strength. The orange circles refer to the surface excess recovered using the Gibbs isotherm and the blue squares indicate the excess sorption normalized by the surface area of the interface. These different approaches generate roughly similar values that are well within the same order of magnitude. This indicates that the Gibbs isotherm can be used to estimate sorption at such interfaces in both striped and mixed brushes.

B. Contributions of interfaces to sorption in mixed brushes

Figure 6 displays solvent and polymer density profiles for a selection of mixed brushes from experiment 1 in Table I with a chain fraction ϕ of 0.0, 0.25, and 0.5. These density profiles show the equilibrium distribution of the polymer and solvent after exposing

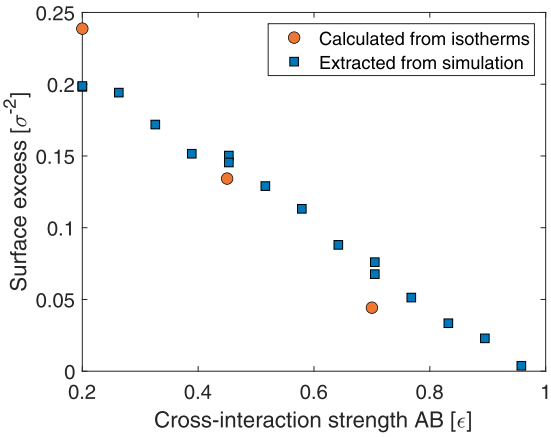

FIG. 5. Surface excess (or sorption at the polymer–polymer interface) decreases with an increasing cross-interaction strength. The values for the surface excess recovered from the Gibbs isotherm (orange circles) match well with the surface adsorption extracted from the simulations (blue squares).

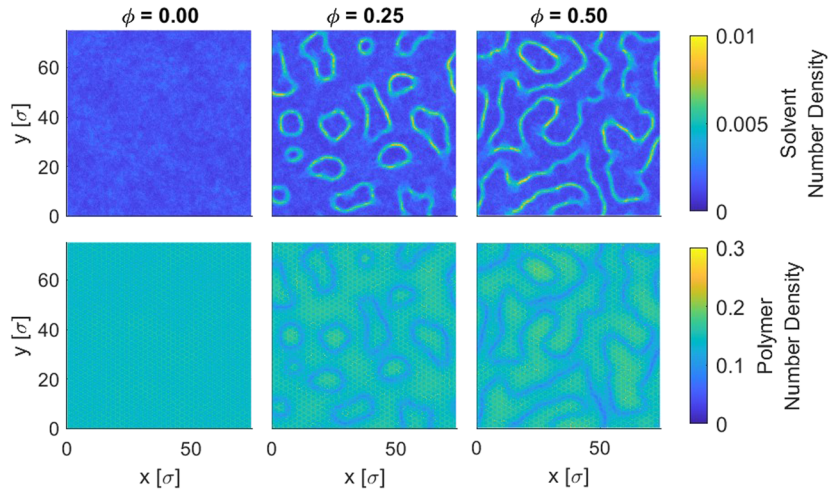

FIG. 6. Projected density profiles of the sorption of vapor in mixed brushes selected chain fractions sampled over 1 M time steps. The relative vapor pressure is 30% and The cross-interaction strength ε_{AB} is 0.453ε. Top row: solvent density profiles. Bottom row: polymer density profile.

mixed brushes with a cross-interaction strength of $\varepsilon_{AB} = 0.453\varepsilon$ to a Lennard-Jones vapor at a relative vapor pressure of 30%. First, we observe that these density profiles show similar sorption behavior compared to what we reported previously:[31] solvent adsorbs especially at interfaces between different polymer domains. If we compare the panels in the top row with those in the bottom row, we observe that a lower local density in the polymer is accompanied by a higher local density of the solvent, indicating adsorption at interfaces. Second, Fig. 6 and the figures in the supplementary material, Sec. 3, show that with an increasing chain fraction, the average domain size grows both by a gradual increase in the size of individual domains and by aggregation of multiple domains into a single domain. The domain structure thus depends on the chain fraction of the mixed brush, and this also affects the polymer–polymer interfacial area: the sorption at the interface should also depend on the chain fraction.

The ratio between the grafted polymers, indeed, has a significant influence on the amount of additional absorption. Figure 7 displays the excess absorption of mixed brushes as a function of the fractions of type A chains in the brush. At a relative vapor pressure of 30% and a cross-interaction strength (ε_{AB}) of 0.453ε, we observe a gradual increase in the absorption when the chain fraction ϕ is increased from 0 to 0.5. More specifically, there is a 0.04 σ^{-2} increase between a pure brush ($\phi = 0$) and a 1:1 mixed brush ($\phi = 0.5$). The behavior of this increase correlates well with the increase in the AB surface area when the chain fraction is increased.

The pair interactions do not change when the chain fraction is changed, so the surface excess can be assumed to be approximately constant. The adsorption should then be linearly related to the surface area between the different phases. The line in Fig. 7 shows this agreement between the theoretical description and the simulations: the surface excess, i.e., the ratio between the sorption and surface area, is 0.0918 σ^{-2}. This is of the same order of magnitude as expected based on the isotherm of a well-defined interface in a striped brush, where it would be 0.08 σ^{-2} (see the supplementary material, Sec. 5). The degree of qualitative agreement between the simulation and model is remarkable, yet there are several slight discrepancies.

First, at lower chain fractions between $\phi = 0.1$ and 0.3, the sorption is underestimated by the model up to 20%. For these low chain fractions, the energetic difference between the half-sphere phase and the cylindrical phase is <1 kT/chain. As a result, both phases coexists and small fluctuations in the local grafting will lead to a local preference of one phase over the other. Globally, this results in a mixed phase that has some half-sphere domains in a majority cylindrical phase. We observe this mixture of phases in the simulation snapshots as well (see the supplementary material, Sec. 6). However, the model only predicts the majority cylindrical phase and its associated interfacial area. Because the half-sphere phase has a higher surface area as the cylindrical phase, this minority phase introduces an additional surface area that is not accounted for in the model, leading to a slight underestimation of the sorption.

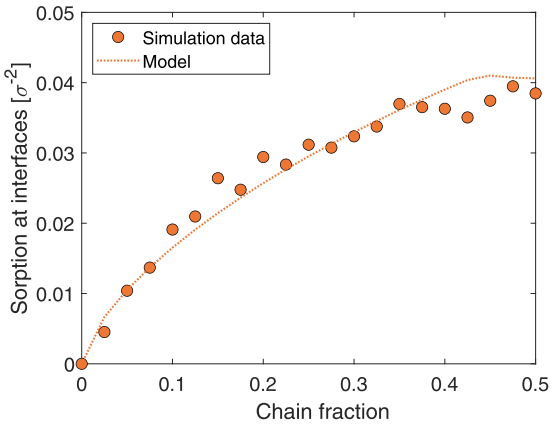

FIG. 7. Sorption of vapor at the polymer–polymer interface for a changing chain fraction ϕ. A higher chain fraction (until $\phi = 0.5$) results in more sorption, which is in line with the expected increase in the surface area between the different phases. At values of ϕ close to 0.5, the sorption levels off because the domains aggregate and form a ripple phase. The expected surface area matches the sorption curve with a scaling factor of 0.0918 σ^{-2}.

Second, the model seems to overestimate sorption around $\phi = 0.4$ by ~15%. This is the result of how we describe the ripple phase in the model. In the model, this phase is represented by straight lines, whereas it has a meandering character (see also Fig. 6) in the simulations. This meandering character is the result of domain aggregation; when the cylindrical domains increase with increasing chain fraction, they start to overlap and aggregate. This aggregation is not captured in the model, which leads to an overestimation of the sorption near the phase transition between the cylindrical and ripple phases.

Another brush property that influences the sorption at the interface is the grafting density. A higher grafting density results in more polymer on the same surface area and thus leads to an increased brush height. The interfaces in the cylindrical and ripple phase scale with this height. Figure 8 displays the sorption at the polymer–polymer interface as a function of the grafting density for a mixed brush with a 1:1 ratio between A and B chains (experiment 2 in Table I). The sorption at the interface increases with increasing grafting density from $7.7 \cdot 10^{-3}\sigma^{-2}$ at a grafting density of $0.15\sigma^{-2}$ to $65.4 \cdot 10^{-3}\sigma^{-2}$ at a grafting density of $0.35\sigma^{-2}$. At low grafting densities ($< 0.15\sigma^{-2}$), the model is not able to capture this behavior since the model assumes a grafting density well above the critical grafting density. From the polymer density profiles, we observe that the critical grafting density for a pure brush is between 0.10 and 0.15 σ^{-2} and for a mixed brush system, this transition is at slightly higher grafting densities (see the supplementary material, Sec. 4).

Nevertheless, we can extract the qualitative behavior of the interfacial surface area from the model: the interface increases linearly with the grafting density as shown in Eq. (8). The results in Fig. 8 show a similar behavior assuming that the surface excess remains the same. The dotted line in the figure displays a linear fit over the data points above the critical grafting density, giving a slope of 0.288, which is higher than the expected value of 0.16 for the simulation parameters of the brushes in this work. This difference can be partially explained by the straight stripe character of the model compared to the irregular stripes in the simulation. Additionally, the estimates for the stretching length in the model (L_A and L_B) contain assumptions regarding the in-plane contribution based on the domain size: this contribution is assumed to be equal for all chains of a single type. As a result, the model predicts the correct qualitative behavior with a quantitative error.

C. Contributions of pair interactions to sorption in mixed brushes

The total sorption is also affected by the interactions between the different components in the system. In mixed brushes, examples of these interactions include polymer self-interactions and polymer–vapor interactions. In single-component polymer brushes, a stronger self-interaction leads to less vapor sorption[29] and this behavior is qualitatively conserved in the domains of mixed brushes: a stronger self-interaction in either or both phases leads to a reduction in the total sorption in the brush (see the supplementary material, Sec. 7). In fact, the different phases absorb vapor independently of each other as shown by the results from experiment 3 in Table I: for instance, the sorption in a mixed brush with $\varepsilon_{AA} = 0.6$ and $\varepsilon_{BB} = 1.4$ is within 10% of the sorption that would be expected by summing the contribution of each phase based on mixed brushes with $\varepsilon_{AA} = \varepsilon_{BB} = 0.6$ and $\varepsilon_{AA} = \varepsilon_{BB} = 1.4$. This indicates that the adsorption at the interface is not significantly affected by the polymer self-interaction.

Besides these self-interactions, total sorption is also influenced by the polymer–vapor interaction. Figure 9 shows the effect of this polymer–vapor interaction on the sorption in mixed brushes with $\phi = 0.5$ for experiment 4 in Table I. We note that the systems are phase separated for all interaction strengths that were evaluated in these simulations. Generally, the stronger the polymer–vapor interaction, the higher the sorption at the interface. For a large part, this trend can be explained by the contribution of bulk sorption to the total sorption. However, contrary to the polymer self-interaction, the polymer–vapor interaction strength does affect the sorption at the interface. To illustrate, we note that a mixed brush with $\varepsilon_{AS} = 0.6$

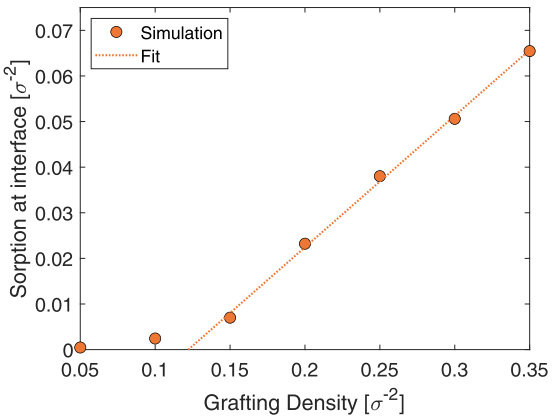

FIG. 8. Interfacial sorption (or surface) excess for mixed brushes with varying grafting densities and $\phi = 0.5$. A higher grafting density leads to a linear increase in the surface area according to the free-energy model; the linear fit of the data points above the critical grafting density show a qualitative agreement between the model and the simulation.

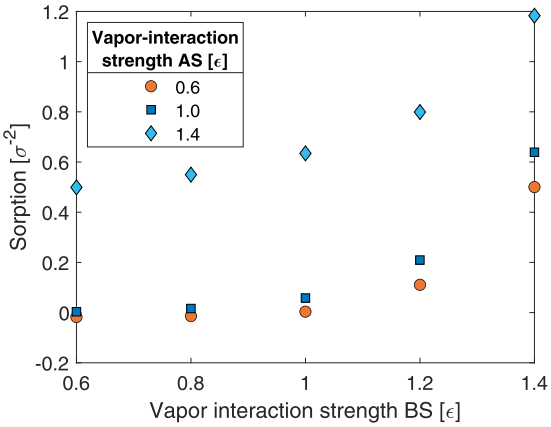

FIG. 9. Total sorption of vapor in a mixed brush with $\phi = 0.5$ for different polymer–vapor interaction strengths. A stronger interaction strength leads to more vapor sorption due to additional bulk sorption and interface effects.

and $\varepsilon_{BS} = 1.0$ could be approximated as half a mixed brush where $\varepsilon_{AS} = \varepsilon_{BS} = 0.6$ and half a mixed brush where $\varepsilon_{AS} = \varepsilon_{BS} = 1.0$. If the interfacial sorption was unaffected by the value of ε_{AS} and ε_{BS}, then the sorption in the former and latter systems should be equal. However, we find that the former differs by ~80% compared to the latter (see the supplementary material, Sec. 8) and the only difference between the system and its approximation is the polymer–polymer interface. This indicates that the adsorption at the interface is significantly affected by the polymer–vapor interaction. This difference decreases significantly for higher interaction strengths.

This effect can be understood based on a simple statistical thermodynamical model. If we assume that the interface consists of independent adsorption sites, the system gains energy upon adsorption based on the pair interactions around this interface. Before adsorption, this interface consists of only AB interactions and hence the site-energy around this interface is related to the polymer cross-interaction strength. Upon adsorption, the AB-interface is eliminated and replaced with an A-solvent and a B-solvent interface, giving a site-energy related to both polymer–vapor interaction strengths. The adsorption is then related to the ratio of the Gibbs factors for the empty and filled adsorption sites. The exponential nature of these Gibbs factors make the site occupancy (and thus sorption at the interface) to be susceptible to small changes in the polymer–vapor interaction strength if this interaction strength is close to the cross-interaction strength of the polymers. Conversely, at high polymer–vapor interaction strengths, most sites are already occupied, so a further increase will not result in much additional adsorption.

D. Discussion

In order to optimize the sorption performance of mixed brushes, one should take into account a variety of brush parameters that include the grafting density, chain fraction, polymer cross-interactions, and other pair interactions. To maximize sorption at the polymer–polymer interfaces, a chain fraction of ~0.5 and a grafting density as high as possible are desired. These conditions lead to the most additional interface for this contribution to the total sorption. Additionally, one should strive for a low cross-interaction strength between both polymer components. In essence, this comes down to polymers that do not tend to mix well.

Moreover, the other pair interactions in the system also contribute to the total sorption. Similar to single-component brushes,[29] a lower polymer self-interaction leads to more sorption in the bulk of the domains. This parameter does however not affect the sorption at the interfaces between these domains. Similarly, a stronger polymer–vapor interaction also leads to more bulk sorption. Nevertheless, a higher polymer–vapor interaction also increases the sorption at the interface under conditions of limited bulk sorption when the polymer–vapor interaction is weaker than the polymer self-interaction. Hence, interfacial sorption can enhance adsorption in mixed brushes for limited bulk sorption conditions.

Our simulations clearly indicate an enhanced absorption in binary polymer brushes in vapors. However, the enhanced absorption effect is not limited to binary brushes in vapors: it will work for other systems as well, provided that the background solvent is a poor solvent. In fact, a similar effect has also been observed in liquids.[57] Mixed poly(acrylic acid) (PAA)/poly(*N*-isopropyl acrylamide) (PNIPAAM) brushes showed a higher absorption potential for human serum albumin than either pure PAA or pure PNIPAAM brushes. Hence, this effect may prove relevant for sensors in liquids as well.

The systems studied in this article provide an opportunity to increase the sensitivity of sensor platforms by increasing the vapor uptake. Yet, an equally important property of coatings is the selectivity to particular groups of molecules. We have recently shown that the absorption in homopolymer brushes of one type of vapor can interfere with the absorption of a second type of vapor.[30] Therefore, one can anticipate non-trivial effects for the absorption of vapor mixtures in binary brushes as well. In particular, since one can expect that cosolvency[58] and cononsolvency[59,60] effects can occur for vapor mixtures as well,[28] these effects are known to allow for exotic structures in double responsive polymers.[61]

Finally, we would like to highlight that the concept presented here might find application in systems beyond sensor platforms. For example, membrane technologies can be tuned by sorption processes as well.[62] By grafting membrane pores with end-grafted polymers, target gases can be separated[63] and the binary brush systems might give rise to molecular highways for more effective gas separations.

In conclusion, we evaluated the sorption characteristics of polymer–polymer interfaces in binary polymer brushes and found that this adsorption follows the Gibbs adsorption isotherm. We developed a free-energy model to estimate the polymer–polymer interface area of a mixed polymer brush and showed that this interface area is related to the sorption at this interface with a proportionality constant, the surface excess. This more detailed understanding of these polymer–polymer brushes introduces some design parameters for the use of such coatings in sensing and separation applications.

SUPPLEMENTARY MATERIAL

See the supplementary material for determination of surface tension, simulation details of mixed brushes, particle density profiles for varying chain fraction, particle density profiles for varying grafting density, snapshots of phase coexistence, effect on sorption of self-interaction of polymer phases, and effect on sorption of polymer–vapor interaction of polymer phases.

ACKNOWLEDGMENTS

We thank W. K. den Otter for critical reading of the manuscript and acknowledge NWO and SURFsara for HPC resources and support (Project No. EINF-700). This work was part of the research program "Mechanics of Moist Brushes" with Project No. OCENW.KLEIN.020, which is financed by the Dutch Research Council (NWO).

DATA AVAILABILITY

The data that support the findings of this study are openly available in the 4.TU Data Center at http://doi.org/10.4121/14560605.

REFERENCES

[1]P. G. de Gennes, "Conformations of polymers attached to an interface," Macromolecules **13**, 1069–1075 (1980).
[2]S. T. Milner, "Polymer brushes," Science **251**, 905–914 (1991).
[3]W.-L. Chen, R. Cordero, H. Tran, and C. K. Ober, "*50th Anniversary Perspective*: Polymer brushes: Novel surfaces for future materials," Macromolecules **50**, 4089–4113 (2017).
[4]Y. Yu, M. Brió Pérez, C. Cao, and S. de Beer, "Switching (bio-) adhesion and friction in liquid by stimulus responsive polymer coatings," Eur. Polym. J. **147**, 110298 (2021).
[5]M. Chen, W. H. Briscoe, S. P. Armes, and J. Klein, "Lubrication at physiological pressures by polyzwitterionic brushes," Science **323**, 1698–1701 (2009).
[6]Y. Higaki, M. Kobayashi, D. Murakami, and A. Takahara, "Anti-fouling behavior of polymer brush immobilized surfaces," Polym. J. **48**, 325–331 (2016).
[7]E. M. Benetti and N. D. Spencer, "Using polymers to impart lubricity and biopassivity to surfaces: Are these properties linked?," Helv. Chim. Acta **102**, e1900071 (2019).
[8]J. O. Zoppe, N. C. Ataman, P. Mocny, J. Wang, J. Moraes, and H.-A. Klok, "Surface-initiated controlled radical polymerization: State-of-the-art, opportunities, and challenges in surface and interface engineering with polymer brushes," Chem. Rev. **117**, 1105–1318 (2017).
[9]H. Merlitz, G.-L. He, C.-X. Wu, and J.-U. Sommer, "Nanoscale brushes: How to build a smart surface coating," Phys. Rev. Lett. **102**, 115702 (2009).
[10]M. Welch, A. Rastogi, and C. Ober, "Polymer brushes for electrochemical biosensors," Soft Matter **7**, 297–302 (2011).
[11]L. I. Klushin, A. M. Skvortsov, A. A. Polotsky, S. Qi, and F. Schmid, "Sharp and fast: Sensors and switches based on polymer brushes with adsorption-active minority chains," Phys. Rev. Lett. **113**, 068303 (2014).
[12]S. Qi, L. I. Klushin, A. M. Skvortsov, M. Liu, J. Zhou, and F. Schmid, "Tuning transition properties of stimuli-responsive brushes by polydispersity," Adv. Funct. Mater. **28**, 1800745 (2018).
[13]M. Koch, D. Romeis, and J.-U. Sommer, "End-adsorbing chains in polymer brushes: Pathway to highly metastable switchable surfaces," Macromolecules **53**, 7356–7368 (2020).
[14]V. Parrillo, A. de los Santos Pereira, T. Riedel, and C. Rodriguez-Emmenegger, "Catalyst-free 'click' functionalization of polymer brushes preserves antifouling properties enabling detection in blood plasma," Anal. Chim. Acta **971**, 78–87 (2017).
[15]A. R. Kuzmyn, A. T. Nguyen, H. Zuilhof, and J. Baggerman, "Bioactive antifouling surfaces by visible-light-triggered polymerization," Adv. Mater. Interfaces **6**, 1900351 (2019).
[16]M. A. Cohen Stuart, W. T. S. Huck, J. Genzer, M. Müller, C. Ober, M. Stamm, G. B. Sukhorukov, I. Szleifer, V. V. Tsukruk, M. Urban, F. Winnik, S. Zauscher, I. Luzinov, and S. Minko, "Emerging applications of stimuli-responsive polymer materials," Nat. Mater. **9**, 101 (2010).
[17]D. Mukherji, C. M. Marques, and K. Kremer, "Smart responsive polymers: Fundamentals and design principles," Annu. Rev. Condens. Matter Phys. **11**, 271–299 (2020).
[18]L. Li, J. Li, and C. M. Lukehart, "Graphitic carbon nanofiber-poly(acrylate) polymer brushes as gas sensors," Sens. Actuators, B **130**, 783–788 (2008).
[19]H. C. McCaig, E. Myers, N. S. Lewis, and M. L. Roukes, "Vapor sensing characteristics of nanoelectromechanical chemical sensors functionalized using surface-initiated polymerization," Nano Lett. **14**, 3728–3732 (2014).
[20]R. J. Horst, M. Brió Pérez, R. Cohen, M. Cirelli, P. S. Dueñas Robles, M. G. Elshof, A. Andreski, M. A. Hempenius, N. E. Benes, C. Damen, and S. de Beer, "Swelling of poly(methyl acrylate) brushes in acetone vapor," Langmuir **36**, 12053–12060 (2020).
[21]H. Nazemi, A. Joseph, J. Park, and A. Emadi, "Advanced micro- and nano-gas sensor technology: A review," Sensors **19**, 1285 (2019).
[22]M. Biesalski and J. Rühe, "Swelling of a polyelectrolyte brush in humid air," Langmuir **16**, 1943–1950 (2000).
[23]C. J. Galvin, M. D. Dimitriou, S. K. Satija, and J. Genzer, "Swelling of polyelectrolyte and polyzwitterion brushes by humid vapors," J. Am. Chem. Soc. **136**, 12737–12745 (2014).
[24]C. J. Galvin and J. Genzer, "Swelling of hydrophilic polymer brushes by water and alcohol vapors," Macromolecules **49**, 4316–4329 (2016).
[25]M. Brió Pérez, M. Cirelli, and S. de Beer, "Degrafting of polymer brushes by exposure to humid air," ACS Appl. Polym. Mater. **2**, 3039–3043 (2020).
[26]E. Aliyev, S. Shishatskiy, C. Abetz, Y. J. Lee, S. Neumann, T. Emmler, and V. Filiz, "SI-ATRP polymer-functionalized graphene oxide for water vapor separation," Adv.Mater. Interfaces **7**, 2000443 (2020).
[27]L. P. Kreuzer, C. Lindenmeir, C. Geiger, T. Widmann, V. Hildebrand, A. Laschewsky, C. M. Papadakis, and P. Müller-Buschbaum, "Poly(sulfobetaine) versus poly(*N*-isopropylmethacrylamide): Co-nonsolvency-type behavior of thin films in a water/methanol atmosphere," Macromolecules **54**, 1548–1556 (2021).
[28]C. Geiger, J. Reitenbach, L. P. Kreuzer, T. Widmann, P. Wang, R. Cubitt, C. Henschel, A. Laschewsky, C. M. Papadakis, and P. Müller-Buschbaum, "PMMA-*b*-PNIPAM thin films display cononsolvency-driven response in mixed water/methanol vapors," Macromolecules **54**, 3517–3530 (2021).
[29]G. C. Ritsema van Eck, L. B. Veldscholte, J. H. W. H. Nijkamp, and S. de Beer, "Sorption characteristics of polymer brushes in equilibrium with solvent vapors," Macromolecules **53**, 8428–8437 (2020).
[30]L. A. Smook, G. C. Ritsema van Eck, and S. de Beer, "Friends, foes, and favorites: Relative interactions determine how polymer brushes absorb vapors of binary solvents," Macromolecules **53**, 10898–10906 (2020).
[31]L. A. Smook, G. C. Ritsema van Eck, and S. de Beer, "Concentrating vapor traces with binary brushes of immiscible polymers," ACS Appl. Polym. Mater. **3**, 2336–2340 (2021).
[32]L. Wang, T. Zhong, X. Quan, and J. Zhou, "Solvent-responsiveness of PS-PEO binary mixed polymer brushes: A coarse-grained molecular dynamics study," Mol. Simul. **43**, 1322–1330 (2017).
[33]M. Li and C. W. Pester, "Mixed polymer brushes for 'smart' surfaces," Polymers **12**, 1553 (2020).
[34]M. Kumar Vyas, K. Schneider, B. Nandan, and M. Stamm, "Switching of friction by binary polymer brushes," Soft Matter **4**, 1024–1032 (2008).
[35]X. Sui, S. Zapotoczny, E. M. Benetti, M. Memesa, M. A. Hempenius, and G. J. Vancso, "Grafting mixed responsive brushes of poly(*N*-isopropylacrylamide) and poly(methacrylic acid) from gold by selective initiation," Polym. Chem. **2**, 879–884 (2011).
[36]W. Wei, T.-Y. Kim, A. Balamurugan, J. Sun, R. Chen, A. Ghosh, F. Rodolakis, J. L. McChesney, A. Lakkham, P. G. Evans, S.-M. Hur, and P. Gopalan, "Phase behavior of mixed polymer brushes grown from ultrathin coatings," ACS Macro Lett. **8**, 1086–1090 (2019).
[37]J. Wang and M. Müller, "Microphase separation of mixed polymer brushes: Dependence of the morphology on grafting density, composition, chain-length asymmetry, solvent quality, and selectivity," J. Phys. Chem. B **113**, 11384–11402 (2009).
[38]S. Santer, A. Kopyshev, J. Donges, J. Rühe, X. Jiang, B. Zhao, and M. Müller, "Memory of surface patterns in mixed polymer brushes: Simulation and experiment," Langmuir **23**, 279–285 (2007).
[39]A. D. Price, S.-M. Hur, G. H. Fredrickson, A. L. Frischknecht, and D. L. Huber, "Exploring lateral microphase separation in mixed polymer brushes by experiment and self-consistent field theory simulations," Macromolecules **45**, 510–524 (2012).
[40]K. Gong and W. G. Chapman, "Solvent response of mixed polymer brushes," J. Chem. Phys. **135**, 214901 (2011).
[41]G.-L. He, H. Merlitz, J.-U. Sommer, and C.-X. Wu, "Microphase separation of mixed binary polymer brushes at different temperatures," Macromolecules **42**, 7194–7202 (2009).
[42]N. Akkilic, F. A. M. Leermakers, and W. M. de Vos, "Responsive polymer brushes for controlled nanoparticle exposure," Nanoscale **7**, 17871–17878 (2015).
[43]I. Bos, H. Merlitz, A. Rosenthal, P. Uhlmann, and J.-U. Sommer, "Design of binary polymer brushes with tuneable functionality," Soft Matter **14**, 7237–7245 (2018).
[44]The chemical potential of vapor can be used to calculate the vapor pressure of this vapor. For an ideal gas, this calculated pressure is equal to the measured vapor pressure. For a non-ideal gas, this calculated vapor pressure differs from the measured vapor pressure. This calculated vapor pressure is the fugacity.

[45]S.-M. Hur, A. L. Frischknecht, D. L. Huber, and G. H. Fredrickson, "Self-consistent field simulations of self- and directed-assembly in a mixed polymer brush," Soft Matter **7**, 8776–8788 (2011).
[46]S.-M. Hur, A. L. Frischknecht, D. L. Huber, and G. H. Fredrickson, "Self-assembly in a mixed polymer brush with inhomogeneous grafting density composition," Soft Matter **9**, 5341–5354 (2013).
[47]C. Singh, E. B. Zhulina, D. Gersappe, G. T. Pickett, and A. C. Balazs, "A 'jumping micelle' phase transition," Macromolecules **29**, 7637–7640 (1996).
[48]C. Singh, G. T. Pickett, and A. C. Balazs, "Interactions between polymer-coated surfaces in poor solvents. 1. Surfaces grafted with A and B homopolymers," Macromolecules **29**, 7559–7570 (1996).
[49]K. Kremer and G. S. Grest, "Dynamics of entangled linear polymer melts: A molecular-dynamics simulation," J. Chem. Phys. **92**, 5057 (1990).
[50]A. Galuschko, L. Spirin, T. Kreer, A. Johner, C. Pastorino, J. Wittmer, and J. Baschnagel, "Frictional forces between strongly compressed, nonentangled polymer brushes: Molecular dynamics simulations and scaling theory," Langmuir **26**, 6418–6429 (2010).
[51]S. De Beer, E. Kutnyanszky, P. M. Schön, G. J. Vancso, and M. H. Müser, "Solvent-induced immiscibility of polymer brushes eliminates dissipation channels," Nat. Commun. **5**, 3781 (2014).
[52]M. K. Singh, P. Ilg, R. M. Espinosa-Marzal, M. Kröger, and N. D. Spencer, "Polymer brushes under shear: Molecular dynamics simulations compared to experiments," Langmuir **31**, 4798–4805 (2015).
[53]E. Braun, S. M. Moosavi, and B. Smit, "Anomalous effects of velocity rescaling algorithms: The flying ice cube effect revisited," J. Chem. Theory Comput. **14**, 5262–5272 (2018).
[54]M. Tuckerman, B. J. Berne, and G. J. Martyna, "Reversible multiple time scale molecular dynamics," J. Chem. Phys. **97**, 1990–2001 (1992).
[55]D. Mukherji and K. Kremer, "Coil–globule–coil transition of PNIPAm in aqueous methanol: Coupling all-atom simulations to semi-grand canonical coarse-grained reservoir," Macromolecules **46**, 9158–9163 (2013).
[56]S. Plimpton, "Fast parallel algorithms for short-range molecular dynamics," J. Comput. Phys. **117**, 1 (1995).
[57]E. Bittrich, M. Kuntzsch, K.-J. Eichhorn, and P. Uhlmann, "Complex pH- and temperature-sensitive swelling behavior of mixed polymer brushes," J. Polym. Sci., Part B: Polym. Phys. **48**, 1606–1615 (2010).
[58]D. Mukherji, C. M. Marques, T. Stuehn, and K. Kremer, "Depleted depletion drives polymer swelling in poor solvent mixtures," Nat. Commun. **8**, 1374 (2017).
[59]D. Mukherji, C. M. Marques, and K. Kremer, "Polymer collapse in miscible good solvents is a generic phenomenon driven by preferential adsorption," Nat. Commun. **5**, 4882 (2014).
[60]A. Galuschko and J.-U. Sommer, "Co-nonsolvency response of a polymer brush: A molecular dynamics study," Macromolecules **52**, 4120–4130 (2019).
[61]D. Mukherji, M. D. Watson, S. Morsbach, M. Schmutz, M. Wagner, C. M. Marques, and K. Kremer, "Soft and smart: Co-nonsolvency-based design of multiresponsive copolymers," Macromolecules **52**, 3471–3478 (2019).
[62]J. J. Keating, J. Imbrogno, and G. Belfort, "Polymer brushes for membrane separations: A review," ACS Appl. Mater. Interfaces **8**, 28383–28399 (2016).
[63]M.-A. Pizzoccaro-Zilamy, M. Drobek, E. Petit, C. Totée, G. Silly, G. Guerrero, M. G. Cowan, A. Ayral, and A. Julbe, "Initial steps toward the development of grafted ionic liquid membranes for the selective transport of CO_2," Ind. Eng. Chem. Res. **57**, 16027–16040 (2018).